Retraction

Retracted: Wireless Network of Silver Film Lysozyme Aptasensor Based on Fractal Measurement

Security and Communication Networks

This article has been retracted by Hindawi, as publisher, following an investigation undertaken by the publisher [1]. This investigation has uncovered evidence of systematic manipulation of the publication and peer-review process. We cannot, therefore, vouch for the reliability or integrity of this article.

Please note that this notice is intended solely to alert readers that the peer-review process of this article has been compromised.

Wiley and Hindawi regret that the usual quality checks did not identify these issues before publication and have since put additional measures in place to safeguard research integrity.

We wish to credit our Research Integrity and Research Publishing teams and anonymous and named external researchers and research integrity experts for contributing to this investigation.

The corresponding author, as the representative of all authors, has been given the opportunity to register their agreement or disagreement to this retraction. We have kept a record of any response received.

References

[1] Z. Wang and M. Wang, "Wireless Network of Silver Film Lysozyme Aptasensor Based on Fractal Measurement," *Security and Communication Networks*, vol. 2021, Article ID 7634982, 9 pages, 2021.

WILEY | Hindawi

Research Article

Wireless Network of Silver Film Lysozyme Aptasensor Based on Fractal Measurement

Zhiyou Wang [1,2] **and Maojin Wang**[1,2]

[1]*School of Electronic Communication and Electrical Engineering, Changsha University, Kaifu District, Changsha, China*
[2]*Hunan Engineering Technology Research Center of Optoelectronic Health Detection, Changsha, China*

Correspondence should be addressed to Zhiyou Wang; zywang@ccsu.edu.cn

In this work, we reported a wireless network composed of silver film-based graphene oxide-fluorescence resonance energy transfer (GO-FRET) lysozyme aptasensor nodes. At the sensor node level, we optimized silver substrate structure, concentrations of the aptamers, and graphene oxide and tested lysozyme detection performance with a model analyte. At the network level, we analyzed the complexity and transmission success rate using fractal measurements. We implemented the wireless network composed of the aptasensor with a portable Wi-Fi fluorescent reader. Transmission success rate testing results show that an increase in node hops can promote the rate of transmission success dramatically. When the hop count is larger than 6, the rate of transmission success can reach more than 90% if the transmission failure probability and sleep probability are 0.1 and 0.5, respectively.

1. Introduction

Lysozyme is an antimicrobial enzyme widely found in diverse organisms. Besides the well-known bacteriolytic activity, lysozyme also possesses an antiproliferative effect against cancer and lung fibroblasts [1, 2]. Because its concentration in body fluids rises dramatically owing to types of diseases such as AIDS, cancer, and Alzheimer's disease, lysozyme can be used as a biomarker candidate of the diseases in early diagnosis and point of care testing (POCT) [3–5]. To achieve accurate concentration measurements in POCT applications, lysozyme-sensing devices are required to satisfy the following needs. First, the devices should feature miniaturized size and a high signal-noise ratio to monitor lysozyme concentration change in mobile and noisy scenarios. Lysozyme sensors based on different detection techniques, such as chromatography, immunoassay, electrochemical analysis, and optical methods, have been reported in the last decades [6–9]. Among them, Loncaric reported a USB-based electrochemical lysozyme sensor, which was composed of a potentiostat and I/V converter, an analog/digital converter, and a microcontroller unit [3].

Though a detection limit of 36 nM was reported in the work, further application of the device was hindered by complexity in the configuration. Besides the electrochemical methods, another potential technique candidate is fluorescence resonance energy transfer (FRET). Based on a nonradiative energy transfer phenomenon between two fluorophores in short distances (<10 nm), i.e., FRET effect, the FRET aptasensor uses aptamers as probes of high affinity and specificity in the detection of lysozyme. Because of the advantages of fast response, noncontamination, and high specificity, FRET aptasensor has been extensively exploited in lysozyme detection studies [9–14]. To achieve sensitivity improvement, FRET sensors based on various materials, structures, and probes have been reported [15–19]. Among the materials employed in the FRET sensors, graphene oxide (GO) is most commonly used because of its tunable fluorescent emission efficiency [15–17]. The FRET sensor structures for amplifying fluorescence signals can be divided into two types. One type of structure is metal nanostructure fabricated through the chemical synthesis of nanoparticles and other fabrication technologies [18]. To achieve desirable local enhancement of the electromagnetic field, researchers have to use

complicated processes to realize fine control of the size and shape of the metal nanostructures, which brings difficulties to large-scale production. The other type of structure is metallic films (50–200 nm) physically deposited on glass substrate for large electromagnetic field penetration depth into analyte [19]. To control the distance between the fluorescein and the mirror, a dielectric buffer layer is fabricated on the mirror surface to achieve the regulation of the fluorescence enhancement effect. Compared with metallic nanostructures, the fabrication of metallic mirrors is relatively simple and of high practical value. Among the metallic mirrors, silver thin film, featuring high fluorescence reflectivity and low material cost, is one of the most desirable choices for the mirror structure [20–22]. To overcome the instability limitation of silver material, we reported a single silver film sensing structure named "plain silver slide" with a gold adhesion enhancing layer between the film and substrate adhesion layer [20]. The structure shows reasonable stability for over 10 hours in liquids and shelf life longer than 3 months under regular storage. Thus, high sensitivity of lysozyme detection can be expected if we apply the plain silver structure in FRET aptasensors.

Second, the devices should be easy to deploy and access on a large scale on different floors. With wireless sensor network (WSN) and its expanded technique, the Internet of medical things (IoMT) has been extensively studied in POCT scenes [23–27]. WSN is a type of network composed of several sensor nodes collecting, processing, and transferring information of objects in a specific monitoring area. Compared with the reported portable devices, WSN can carry different sensors and process information in a specified monitoring area by deploying several sensor nodes, which facilitate users greatly [23–25]. Most of the current WSNs are organized by hierarchical structures of sensor nodes, information sink nodes, and a management platform. In this type of WSNs, data are transmitted to the nodes at higher levels until the cluster head [28]. The cluster head then sends the collected data to the base station, Internet, or satellite for transferring to the management platform in the application layer or background part. The hierarchical structure of WSN can lead to the complexity of link connections between adjacent nodes. Thus, research into network complexity is of particular importance, especially in a large-scale network with high demands of resource allocation optimization and efficiency of energy consumption [29]. Currently, fractal dimension is the most critical concept in the analysis, which has been widely employed to analyze the complexity of structure or data in a network by covering the nodes with boxes of specific sizes and numbers [30–33]. Fractal, a common phenomenon in nature, can be defined as a form featuring similarities between the part and the whole of objects [30]. Different types of properties, such as the coverage of sensor nodes and the volume of the network, can be analyzed in the fractal measurements [31]. Wei reported a concept named information dimension to estimate the probability of exploring the information by calculating the ratio of the number of the nodes in the box to the number of nodes in the network. To further consider the effect of physical factors, e.g., transmission failure rate, node sleep rate, and area size, on the information dimension, Fan proposed a data transmission probability fractal model (PFM). In the model, the current status of WSN can be described by the Markov Mode and transition balance equation. The dimension of cluster information transmission, which can be calculated by considering the aforementioned physical factors in the equation, is helpful to adjust network structure and select transform routes in practice [33].

To improve the sensitivity limitation of lysozyme detection and complexity of WSN transmission success rate analysis in potential POCT scenes, we designed and implemented a WSN of lysozyme aptasensor nodes in a bottom-up way. In the network, each node is composed of a silver film-based GO-FRET aptasensor and a WI-FI fluorescent quantitative reader. At the node level, we optimized the detection sensitivity of the GO-FRET lysozyme aptasensor in the node. In the optimization work, we checked the effect of the metallic layers' thicknesses on the electromagnetic field penetration depth of the silver substrate in the Fresnel equation. We also fabricated the silver substrate and optimized concentrations of GO and multiple aptamers. Different from our previous work, the thiol SAM layer is replaced by an end-grafted polymer buffer layer with thickness controlled by surface-initiated polymerization (SIP) reaction. At the network level, we optimized the structural complexity of the WSN and deployed the network in a laboratory condition and tested its performance. Results show that the transmission success rate is more than 90%, which indicates that the WSN composed of lysozyme aptasensor nodes demonstrates potential applicability in POCT practices.

2. Materials and Methods

2.1. Materials. Three types of aptamers, cytochrome C aptamer, lysozyme aptamer, and thrombin aptamer, were synthesized by Beijing Shenggong Biological Engineering Co., Ltd., and the 5′end was labeled with FAM according to [21]. Thrombin, cytochrome C, and lysozyme were all purchased from Sigma-Aldrich Co. (USA). GO was synthesized in the laboratory using Hummer's method [34, 35]. Polyethylene glycol methacrylate (PEGMA) and 2-hydroxyethyl methacrylate (HEMA), monomers for the polymer buffer layer fabrication, were purchased from Sigma-Aldrich. 4-Dimethylaminopyridine (DMAP), dimethylformamide (DMF) (acidifiers during the SIP reaction), dimethyl sulfoxide (DMSO), ethanol (solvents), 2,2′-Bipyridine (Bipy, catalyzer of the SIP reaction) and Acrylic acid (AA) were purchased from Beijing Chemical Industry Co. Ltd. Succinimidyl-ester diazirine (SDA), photocrosslinking reagent, was purchased from Qcbio Science & Technologies Co. Ltd. The BK7 substrate (75 mm × 25 mm) Schott Glass was purchased from Chengdu Guangming Optical Elements Co. Ltd according to our previous work [36]. All of the other reagents of analytical grade were purchased from Beijing Chemical Plant.

2.2. Methods. As described in the flowchart (Figure 1), the reported work of WSN design and implementation is composed of two parts: sensitivity optimization of the silver film-based GO-FRET lysozyme aptasensor at the node level and fractal analysis and deployment of the WSN at the network level. To achieve the highest electromagnetic field penetration depth and ambient distance between the fluorescein and silver substrate in the step of silver structure parameter optimization, we optimized the thicknesses of metallic layers and buffer layer, respectively. Afterward, we also optimized concentrations of the GO and multiple aptamers in the FRET sensor to achieve a desirable fluorescence quenching effect, which is helpful for measurements of the recovery signal during lysozyme detection. In the fractal analysis, the calculation program was developed in Matlab R2014b on a personal computer with an Intel Core i3 3.70-GHz CPU and 4 GB RAM running Windows 7 Ultimate operating system. Details of each step are described separately in the following sections.

2.3. Optimization of Plain Silver Structure. The diagram of the plain silver structure is shown in Figure 2. For different combinations of gold and silver thicknesses, we calculated the reflectivity and resonant angle of the plain silver structure at a wavelength of 400 nm using the Fresnel method [36]. By choosing the incident angle at the resonant angle, we calculated the penetration depth into the analyte layer and selected a combination of the thicknesses with the largest penetration depth as the optimized plain silver structure parameters.

The silver slides were fabricated according to our previous work described in [20, 36]. An electron beam evaporator (BOC Auto500) with a quartz oscillator was employed for the following metal depositions onto the ultrasonically cleaned glass substrates. Evaporation rates of chromium, gold, and silver were 0.01, 0.01, and 0.08 nm/s, respectively. The morphology of the slide was examined by an atomic force microscope (AFM, Dimension icon, Veeco). Afterward, the polymer buffer layer was fabricated by the SIP reaction method. In the method, Bipy and $CuCl_2$ aqueous solutions were mixed to prepare catalyzer reagent. Then, the mixture of HEMA, PEGMA, distilled water, and methanol was mixed as polymerization reaction liquid. In an argon atmosphere, the reagent, polymerization reaction liquid, was mixed with AA, and the silver slides were dipped in the mixture at room temperature. Lastly, the slides were acidified in a mixture of DMF and DMAP by shaking. Further characterization of the carboxyl group density and buffer thickness was implemented under Lambda950 and Sentech SE850DUV ellipsometer, respectively.

2.4. Optimization of GO and Aptamer Concentration. 30 nM lysozyme aptamer was dissolved in TE buffer (pH = 7.4), and 10 μg/mL, 20 μg/mL, and 30 μg/mL GO solutions were sonicated for one hour. The aptamer was added to the above GO solutions separately, followed by incubating in an oven at 90°C for 5 minutes. The mixture was then cooled to room temperature and transferred to the plain silver slide by photocrosslinking in a dual-wavelength ultraviolet LED crosslinker controlled by an Android app through Bluetooth communication (wavelength: 365 nm and 380 nm and power: 5 W). In the photocrosslinking step, the temperature and humidity were recorded as 25°C and 43%, respectively. To ensure immobilization efficiency of the mixture, the irradiation sequence of the photocrosslinking step was set as our previous work [36]. Lastly, the fluorescence intensity was measured under Hitachi F-4500 fluorescence spectrophotometer.

In concentration optimization of multiple aptamers, 75 nM and 100 nM of all the three aptamers were mixed at the concentration ratio of 1 : 1 : 1 in TE buffer separately and added into 50 μg/mL GO solution for concentration optimization after the fluorescence measurements. In the detection of lysozyme, lysozyme solution at concentrations of 350 nM, 175 nM, 87.5 nM, 43.75 nM, 35 nM, and 21 nM was added to the optimized GO-multiple aptamer systems separately and interacted with the aptamers for 30 minutes. Afterward, the fluorescence recovery signal was measured under the Hitachi F-4500 fluorescence spectrophotometer (Japan).

2.5. Fractal Analysis of WSN Information Dimension and Network Scale. The network transmission probability fractal model (PFM) was used to evaluate the effect of the WSN scale on information dimension under conditions described as below [37]. In the fractal measurement of WSN complexity, different numbers of nodes randomly placed in the area are directly connected to a cluster node by a hierarchical protocol. The MAC layer of the network nodes follows the standard of LEACH protocol. The sleep probability f_1 and transmission failure probability of the nodes are set as 0.5–0.8 and 0.5 respectively, while the node density is 0.04.

2.6. Deployment and Transmission Success Rate Test of the WSN. In the experiment, the optimized lysozyme aptasensor was deployed as the node of WSN along with a Wi-Fi fluorescent quantitative reader with a fluorescence response at a wavelength of 550 nm (Dawnsail Biotech, China). The experimental environment is set as our previous work [38]. Briefly, the number of the sensor nodes on each floor is 80 with the node density as 0.05. The communication distance is 30 meters indoors and 80 meters outdoors, respectively. The detection distance of each node is 15 meters.

3. Results and Discussion

3.1. Optimization of Gold and Silver Layer Thicknesses. To optimize the thickness of gold and silver films in the plain silver SEF structure, i.e., a chromium adhesion layer, gold adhesion enhancing layer, silver film, polymer buffer layer, and analyte layer, on the glass substrate from bottom to top, the propagation depth of electromagnetic waves in the analyte layer was calculated according to the Fresnel equation, as shown in Figure 3(a). The results show that the above performance parameters get the optimal values at the thickness of 2 nm for the gold adhesion enhancing layer and
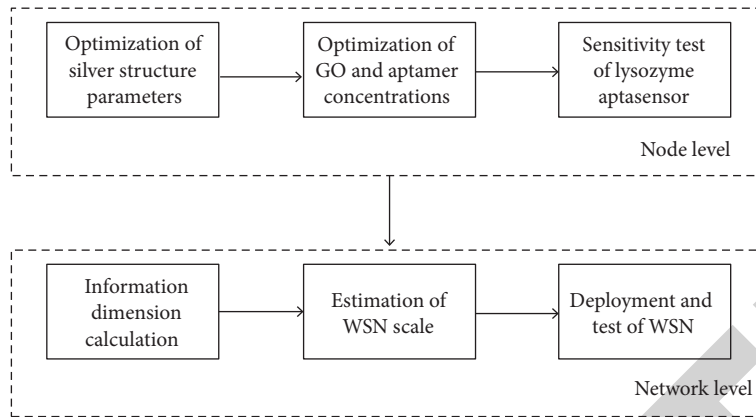
Figure 1: Flowchart of lysozyme aptasensor wireless network design and implementation.
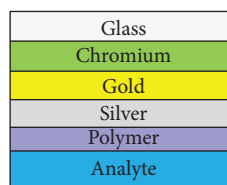

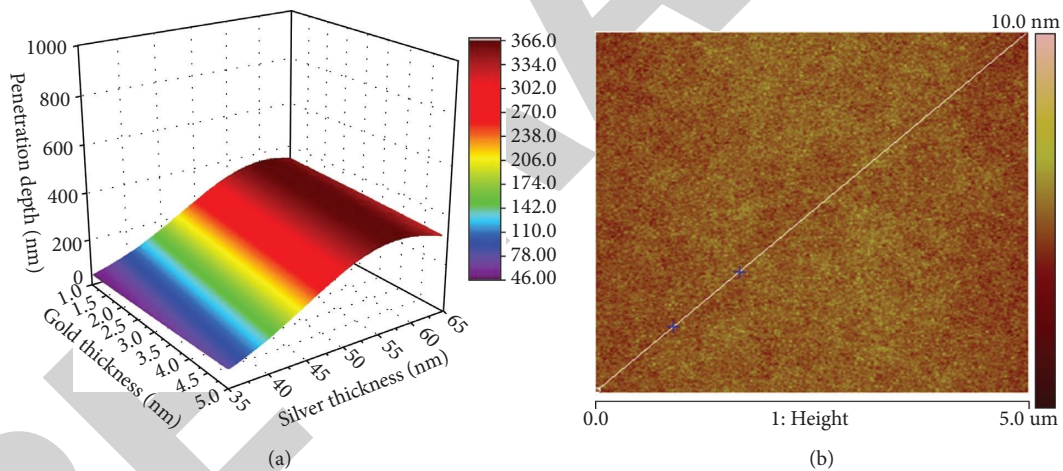Figure 2: Structure diagram of the plain silver substrate.

Figure 3: (a) Penetration depth and (b) AFM characterization of the plain silver substrate.

55 nm for the silver thin film in this paper. Using the above structural parameters, the plain silver structure with a 3 nm chromium adhesion layer was fabricated according to [20]. Physical appearances of the plain silver slide were examined by the AFM, as in Figure 3(b), before fabrication of the buffer layer. The surface roughness of the sensor surface was 0.502 nm, which proves that surface of the plain silver slide is smooth enough for further fabrication of the buffer layer.

Since the fluorescence intensity is very sensitive to the polymer buffer layer thickness, it is necessary to control the polymerization reaction time in the SIP step. For different polymerization reaction duration, carboxyl group density and thickness of the buffer layer were characterized under the near-infrared spectrophotometer and ellipsometer, as in Figures 4(a) and 4(b), respectively. When the carboxyl group density is higher, the peak absorption signal is larger in Figure 4. In the figures, both the carboxyl group density and buffer layer thickness become larger with the increase of the reaction time. According to [19], the best metal enhanced fluorescence can be achieved when the polymer buffer layer thickness is about 10 nm; thus, 5 mins is the optimal reaction duration for the polymerization reaction, as shown in Figure 4(b).

3.2. Optimization of GO and Aptamer Concentration.
When a higher concentration of GO is dissolved in the FRET system, more aptamers can be adsorbed on GO, which is more conducive to quench fluorescence. However, undissolved GO can introduce a fluorescence increment instead
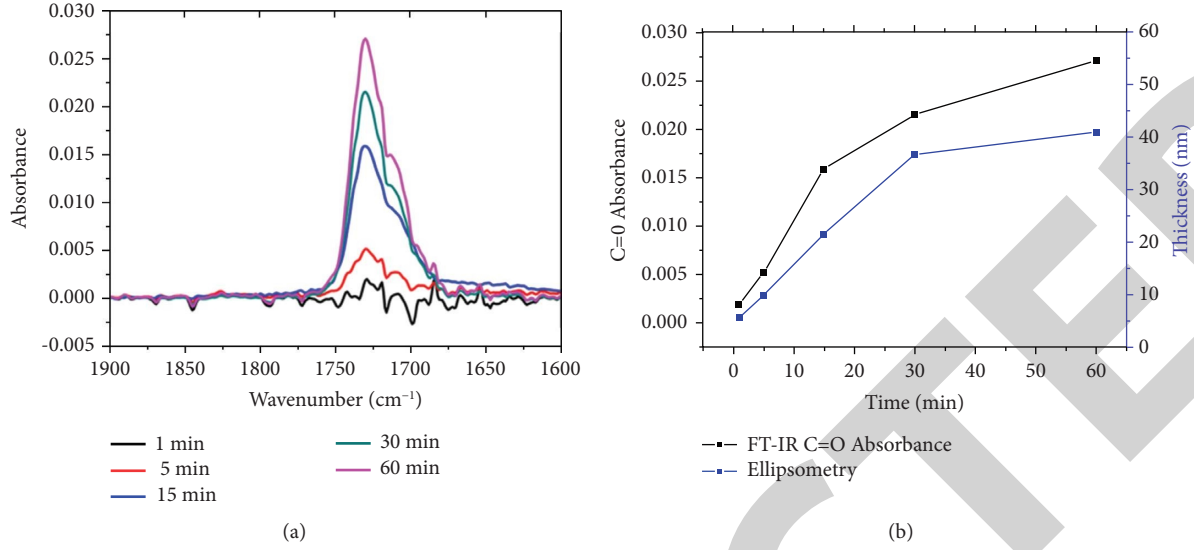
Figure 4: (a) Near-infrared spectrophotometer result and (b) ellipsometer result of the polymer buffer layer.

[39]. Figure 5(a) shows that the desirable fluorescence quenching efficiency can be obtained if we increase GO concentration in the range of 10–20 μg/mL. When the graphene concentration is too high, e.g. 30 μg/mL, the fluorescence value of the FRET system increases. To achieve a high fluorescence quenching efficiency, it is determined that the optimal concentration of GO is 20 μg/mL.

In optimization of the multiple aptamers for fluorescence quenching, with the concentration of GO remaining the same as in the last step, we checked different concentrations of all three aptamers to purchase a high fluorescence quenching efficiency. Compared with 100 nM, the multiple aptamers at 75 nM demonstrated a much higher fluorescence quenching efficiency as in Figure 5(b). Thus, 75 nM is the optimal concentration of multiple aptamers in the GO-FRET detection system.

In the sensitivity test of the silver film-based GO-FRET aptasensor, lysozyme solution at different concentrations was added into the GO-FRET sensors with the optimal concentrations of GO and multiple aptamers separately. In Figure 5(c), the fluorescence signal of the GO-FRET senors increases almost 9 times after recovery when the concentration of lysozyme was 350 nM, which can be explained below. According to [40], lysozyme can interact with GO directly, and the strength of the interaction is stronger than the physical adsorption of aptamers on GO [40]. Thus, all three aptamers fell off from GO because of the specific binding between GO and lysozyme, resulting in a fluorescence recovery phenomenon. After further amplified by the silver substrate, the significant fluorescence recovery signal can be observed as in the figure. Considering baseline noise and fluorescence quenching background in Figure 5(c), the detection limit of the aptasensor was around 30 nM in Figure 5(d), which was comparable with the reported other types of lysozyme sensors [3, 40, 41]. Along with the simplicity of the FRET principle, results of the detection limit comparison show that the proposed silver film-based GO-

FRET aptasensor is suitable as part of the node in WSN. As the number of aptamers increases, fluorescence recovery might continue to improve, and the detection sensitivity of the GO-FRET aptasensor using multiple aptamers can be further promoted.

3.3. Fractal Analysis of WSN Information Dimension and Network Scale. In the PFM of WSN, the "box" covered nodes can be in different states, i.e., sleep, idle, and transmission states according to our previous work [38]. Thus, we firstly divided the WSN area into small square areas S_i (1, 2, ..., N) with a side length l based on the assumption that the nodes cannot be covered by two areas at the same time, and the physical size of the nodes can be ignored compared with the square area. We define the probability of the nodes covered by the area S_i is p_i; then, p_i can be represented by different measurement index d_i in.

$$p_i \approx l^{di} \quad (i = 1, 2, \ldots, N). \tag{1}$$

When the side length l tends to 0, equation (1) can be rewritten as

$$d = \lim_{l \longrightarrow 0} \frac{\ln p_i}{\ln l}. \tag{2}$$

Combined with equation (1), equation (2) can be rewritten as below:

$$D_B \approx \frac{\sum_{i=1}^{n} \ln P_i}{\ln (l)}, \tag{3}$$

where P_i is the probability that a node covered by the square is in a nonsleep state. In the following calculation, we define p as the probability of the node in the transmission state, f as the transmission failure probability, λ as the probability of the node in idle state, q as the probability of the node leaving the link, and μ as the probability of the node in a sleep state.
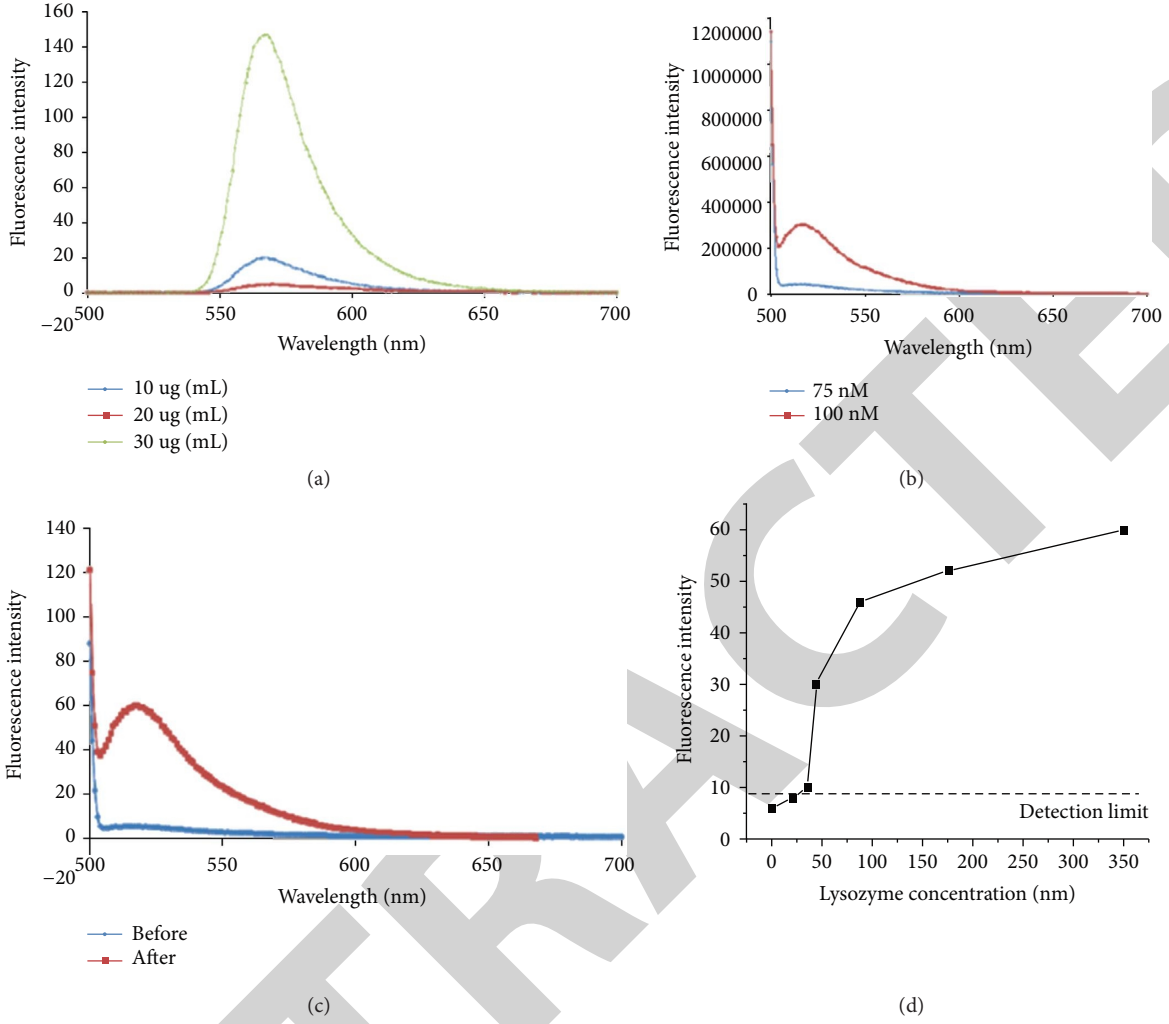
Figure 5: (a) Fluorescence intensity of different GO concentrations, (b) fluorescence intensity of different concentrations of multiple aptamers, (c) fluorescence recovery of 350 nM lysozyme, and (d) sensitivity test of silver film-based GO-FRET aptasensor (fluorescent intensity unit: a.u.).

P_i in equation (4) can be calculated in the transmission balance equation as below:

$$
\left.
\begin{aligned}
&S(0,0) \cdot (3\lambda + 3p) = S(0,1) \cdot f + S(1,0) \cdot q \\
&S(N,M) = \frac{[(K_i - 1)!]^2}{(K_i - 1 - N)!(K_i - 1 - M)!N!M!} \cdot \left(\frac{p}{q}\right)^N \cdot \left(\frac{\lambda}{f}\right)^M \cdot S(0,0), \ (M + N \leq K_i - 1) \\
&P_{K_i}^* = \sum_N S(N,0) \cdot f + \sum_N S(N,1) \cdot f^2 + \cdots + \sum_N S(N, K_i - 1) \cdot (K_i - 1)! \cdot f^{K_i} \\
&P_K = C_K^{K_i} \cdot \mu^{K - K_i} \cdot (1 - \mu)^{K_i} \\
&P_{K_i} = P_K \cdot \left(1 - P_{K_i}^*\right)
\end{aligned}
\right\}.
\tag{4}
$$

In the Matlab calculation, the relationship between the dimension and network size is shown in Figure 6(a). The dimension value becomes larger at the increase of the network scale, while the network size shows an almost
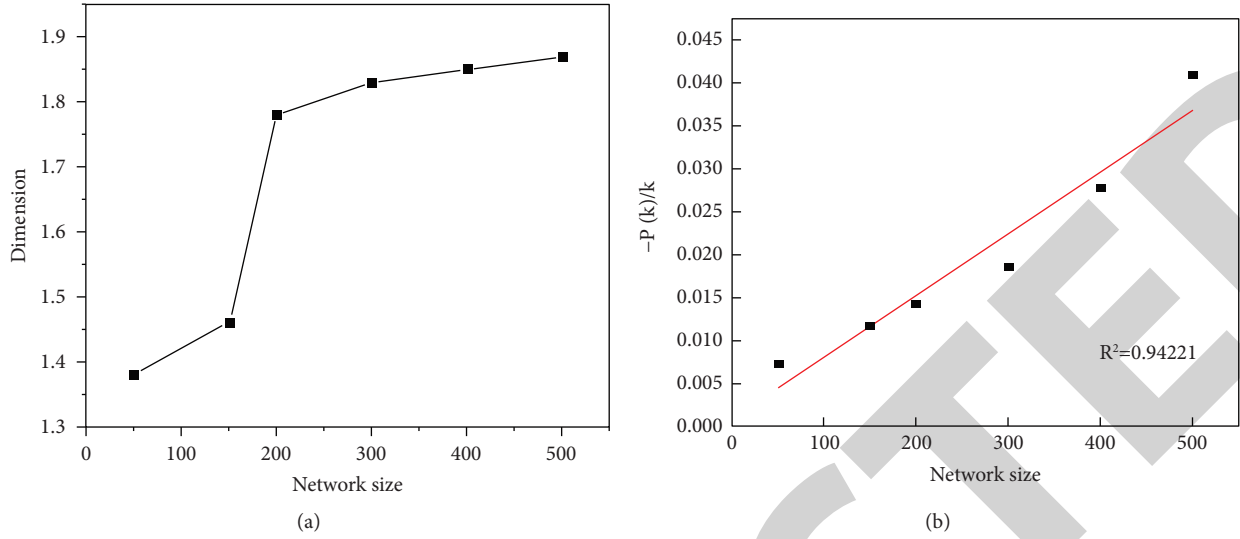
(a)

(b)

Figure 6: Dimension analysis at different network scales, (a) relationship between fractal dimension and number of nodes, and (b) features of probability distribution under different network nodes.
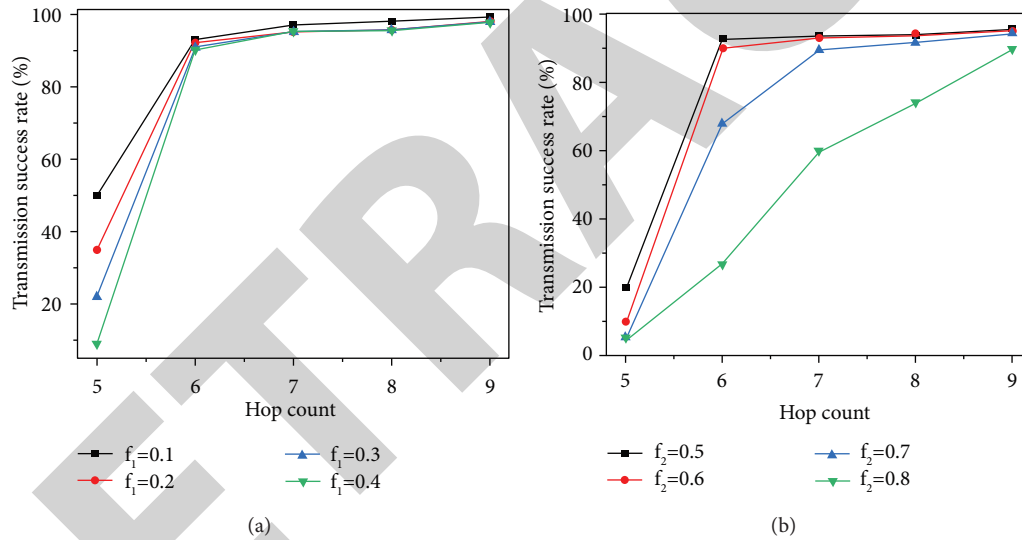

(a)

(b)

Figure 7: Relationship between the hop count number and the success rate of WSN transmission at different failure probabilities (a) and node sleep probabilities (b) of the lysozyme aptasensor node.

linear relationship with the network size when the network size is larger than 200. Besides, although the fractal dimension varies in different scales of the network, the fractal features always exist in the figure. The probability distributions of network degrees of different sizes are further analyzed in Figure 6(b). In the figure, the node degree and the probability of node degree k are distributed around a straight line, and both of them obey the power law. Thus, the complexity of the WSN has fractal self-similarity, which is similar with the reported probability fractal dimension in [33].

3.4. Deployment and Transmission Success Rate Test of the WSN. To test the success rate of the deployed WSN transmission, the number of source-landmark node links was considered at different transmission failures and sleep probabilities of the lysozyme aptasensor nodes. Figure 7(a) shows that, at the transmission, success rate of the WSN can be significantly improved if we control the transmission failure probability of the node at a low level (<0.5) and increase the hop count number in the link. Besides, the increase of the hop count number is also helpful even if a high sleep probability of the node (>0.5)

happens. When the hop count number is larger than 6, if the transmission failure probability of the node is less than 0.5 and the sleep probability of the node is less than 0.7, the transmission success rate can reach more than 90% according to Figure 7(b), which is comparable with our previous work [38].

4. Conclusion

In this work, we reported a WSN composed of silver film-based GO-FRET lysozyme aptasensor nodes by both theoretical analysis and physical implementation. In the design and fabrication of the lysozyme aptasensor nodes, we optimized thicknesses of metallic and buffer layers in the sensor structure by both simulation and experiment. Meanwhile, we optimized concentrations of the multiple aptamers by comparing the fluorescence recovery signal of the sensor and its rival using a single lysozyme aptamer. The experimental results preliminarily show that the fluorescence recovery degree of the GO-FRET sensor using the multiple aptamers is significantly higher than that using the single aptamer during the detection of lysozyme. In the work of WSN design and implementation, we optimized the structural complexity of the WSN by fractal measurements and implemented the aptasensor nodes with a portable Wi-Fi fluorescent reader in laboratory conditions. Testing results of transmission success rate show that when the transmission failure probability is less than 0.5, the sleep probability is smaller than 0.7, and the hop count is larger than 6, the transmission success rate can reach more than 90%. The research fully demonstrates fractal features and applicability of the WSN composed of the silver film-based GO-FRET aptasensor nodes and provides sufficient support for the following research of WSN and IoMT optimization in POCT scenarios.

Data Availability

The experimental data used to support the findings of this study are available from the corresponding author upon request.

Conflicts of Interest

The authors declare that they have no conflicts of interest.

Acknowledgments

References

[1] N. Khan, A. Maddaus, and E. Song, "A low-cost inkjet-printed aptamer-based electrochemical biosensor for the selective detection of lysozyme," *Biosensors*, vol. 8, no. 1, p. 7, 2018.

[2] L. Chen, N. Xia, T. Li, Y. Bai, and X. Chen, "Aptasensor for visual and fluorometric determination of lysozyme based on the inner filter effect of gold nanoparticles on CdTe quantum dots," *Microchim. Acta*, vol. 183, pp. 2917–2923, 2016.

[3] C. Loncaric, Y. Tang, C. Ho, M. A. Parameswaran, and H.-Z. Yu, "A USB-based electrochemical biosensor prototype for point-of-care diagnosis," *Sensors and Actuators B: Chemical*, vol. 161, no. 1, pp. 908–913, 2012.

[4] T. Oeschger, D. McCloskey, V. Kopparthy, A. Singh, and D. Erickson, "Point of care technologies for sepsis diagnosis and treatment," *Lab on a Chip*, vol. 19, no. 5, pp. 728–737, 2019.

[5] L. Helmfors, A. Boman, L. Civitelli et al., A. C. Brorsson and A.-C. Brorsson, Protective properties of lysozyme on β-amyloid pathology: implications for Alzheimer disease," *Neurobiology of Disease*, vol. 83, pp. 122–133, 2015.

[6] M. A. Daeschel, T. Musafija-Jeknic, Y. Wu, D. Bizzarri, and A. Villa, "High-performance liquid chromatography analysis of lysozyme in wine," *American Journal of Enology and Viticulture*, vol. 53, pp. 154–157, 2002.

[7] B. Kerkaert, F. Mestdagh, and B. De Meulenaer, "Detection of hen's egg white lysozyme in food: comparison between a sensitive HPLC and a commercial ELISA method," *Food Chemistry*, vol. 120, pp. 580–584, 2010.

[8] Z. Chen, Q. Xu, G. Tang, S. Liu, S. Xu, and X. Zhang, "A facile electrochemical aptasensor for lysozyme detection based on target-induced turn-off of photosensitization," *Biosensors and Bioelectronics*, vol. 126, pp. 412–417, 2019.

[9] N. G. Walter, "Structural dynamics of catalytic RNA highlighted by fluorescence resonance energy transfer," *Methods*, vol. 25, pp. 19–30, 2001.

[10] R. Roy, S. Hohng, and T. Ha, "A practical guide to single-molecule FRET," *Nature Methods*, vol. 5, pp. 507–516, 2008.

[11] A. Robinson and A. M. van Oijen, "Bacterial replication, transcription and translation: mechanistic insights from single-molecule biochemical studies," *Nature Reviews Microbiology*, vol. 11, pp. 303–315, 2013.

[12] Z. S. Pehlivan, M. Torabfam, H. Kurt, C. O. Yang, N. Hildebrandt, and M. Yuce, "Aptamer and nanomaterial based FRET biosensors: a review on recent advances," *Microchimica Acta*, vol. 186, p. 563, 2019.

[13] K. Sapkota and S. Dhakal, "FRET-based aptasensor for the selective and sensitive detection of lysozyme," *Sensors*, vol. 20, p. 914, 2020.

[14] F. Zhang, S. Wang, and J. Liu, "Gold nanoparticles adsorb DNA and aptamer probes too strongly and a comparison with graphene Oxide for biosensing," *Analytical Chemistry*, vol. 91, pp. 14743–14750, 2019.

[15] M. Arvand and A. A. Mirroshandel, "An efficient fluorescence resonance energy transfer system from quantum dots to graphene oxide nano sheets: application in a photoluminescence aptasensing probe for the sensitive detection of diazinon," *Food Chemistry*, vol. 280, pp. 115–122, 2019.

[16] S. Batabyal, A. Makhal, K. Das, A. K. Raychaudhuri, and S. K. Pal, "Ultrafast dynamics of excitons in semiconductor quantum dots on a plasmonically active nano-structured silver film," *Nanotechnology*, vol. 22, Article ID 195704, 2011.

[17] X. Liu, Y. Wu, X. Wu, and J. X. Zhao, "A graphene oxide-based fluorescence assay for the sensitive detection of DNA exonuclease enzymatic activity," *Analyst*, vol. 144, pp. 6231–6239, 2019.

[18] O. S. Wolfbeis, "An overview of nanoparticles commonly used in fluorescent bioimaging," *Chemical Society Reviews*, vol. 44, pp. 4743–4768, 2015.

[19] T. Harashima, M. Yasuda, and T. Akimoto, "Enhanced fluorescence using an optical interference mirror overlaid

with silver island film," *Analytical Letters*, vol. 47, pp. 2731–2739, 2014.

[20] Z. Cheng, Z. Wang, D. E. Gillespie et al., "Plain silver surface plasmon resonance for microarray application," *Analytical Chemistry*, vol. 87, pp. 1466–1469, 2015.

[21] Z. Wang, Z. Cheng, V. Singh et al., "Stable and sensitive silver surface plasmon resonance imaging sensor using trilayered metallic structures," *Analytical Chemistry*, vol. 86, pp. 1430–1436, 2015.

[22] K. Yano and A. Iwasaki, "Enhancement of fluorescence-based sandwich immunoassay using multilayered microplates modified with plasma-polymerized films," *Sensors*, vol. 17, p. 37, 2017.

[23] C. Zhan, Y. Zeng, and R. Zhang, "Energy-efficient data collection in UAV enabled wireless sensor network," *IEEE Wireless Communications Letters*, vol. 7, pp. 328–331, 2017.

[24] B. Wang, X. Gu, L. Ma, and S. Yan, "Temperature error correction based on BP neural network in meteorological wireless sensor network," *International Journal of Sensor Networks*, vol. 23, no. 4, pp. 265–278, 2017.

[25] S. Jain, M. Nehra, R. Kumar et al., "Internet of medical things (IoMT)-integrated biosensors for point-of-care testing of infectious diseases," *Biosensors and Bioelectronics*, vol. 179, Article ID 113074, 2021.

[26] S. Nayak, N. R. Blumenfeld, T. Laksanasopin, and S. K. Sia, "Point-of-Care diagnostics: recent developments in a connected age," *Analytical Chemistry*, vol. 89, pp. 102–123, 2017.

[27] D. C. Christodouleas, B. Kaur, and P. Chorti, "From point-of-care testing to eHealth diagnostic devices (eDiagnostics)," *ACS Central Science*, vol. 4, pp. 1600–1616, 2018.

[28] J. Wang, Y. Gao, W. Liu, A. Sangaiah, and H.-J. Kim, "An improved routing schema with special clustering using PSO algorithm for heterogeneous wireless sensor network," *Sensors*, vol. 19, no. 3, p. 671, 2019.

[29] M. Ndiaye, G. P. Hancke, and A. M. Abu-Mahfouz, "Software defined networking for improved wireless sensor network management: a survey," *Sensors*, vol. 17, no. 5, p. 1031, 2017.

[30] C. Song, S. Havlin, and H. A. Makse, "Self-similarity of complex networks," *Nature*, vol. 433, p. 392, 2005.

[31] Y. W. Kuo, C. L. Li, J. H. Jhang, and S. Lin, "Design of a wireless sensor network-based IoT platform for wide area and heterogeneous applications," *IEEE Sensors Journal*, vol. 18, no. 12, pp. 5187–5197, 2018.

[32] D. Wei, B. Wei, Y. Hu, H. Zhang, and Y. Deng, "A new information dimension of complex networks," *Physics Letters A*, vol. 378, p. 1091, 2014.

[33] C. Fan, T. Dong, Z. Wen, and Q. Wu, "A low energy algorithm of wireless sensor networks based on fractal dimension," in *Proceedings of the 2016 IEEE International Conference on Network Infrastructure and Digital Content*, pp. 455–459, IC-NIDC), Beijing, China, September 2016.

[34] W. S. Hummers and R. E. Offeman, "Preparation of graphitic oxide," *Journal of the American Chemical Society*, vol. 80, p. 1339, 1958.

[35] S. Senapati, D. K. Patel, B. Ray, and P. Maiti, "Fluorescent-functionalized graphene oxide for selective labeling of tumor cells," *Journal of Biomedical Materials Research Part A*, vol. 107, pp. 1917–1924, 2019.

[36] Z. Wang and M. Wang, "Design and implementation of A miniaturized ultraviolet crosslinker," in *Proceedings of the 4th IEEE International Conference on Knowledge Innovation and Invention*, pp. 54–57, Taichung, Taiwan, July 2021.

[37] A. Khasawneh, M. S. B. Latiff, O. Kaiwartya, and H. Chizari, "A reliable energy-efficient pressure-based routing protocol for underwater wireless sensor network," *Wireless Networks*, vol. 24, no. 6, pp. 2061–2075, 2018.

[38] Z. Wang, Y. Zhou, A. S. Bajenaid, and Y. Chen, *Design of Wireless Sensor Network Using Statistical Fractal Measurements*, Fractals.

[39] J. Shi, J. Guo, G. Bai et al., "A graphene oxide based fluorescence resonance energy transfer (FRET) biosensor for ultrasensitive detection of botulinum neurotoxin A (BoNT/A) enzymatic activity," *Biosensors and Bioelectronics*, vol. 65, pp. 238–244, 2015.

[40] Z. Yang, L. Qin, D. Yang, Q. Hu, and J. Jin, "A graphene oxide fluorescent sensing platform for sensitive and specific detecting biomarker of radiation-resistant nasopharyngeal carcinoma," *Bioorganic & Medicinal Chemistry Letters*, vol. 29, pp. 2383–2386, 2019.

[41] J. F. Wu, X. Gao, L. Ge, G. C. Zhao, and G. F. Wang, "A fluorescence sensing platform of theophylline based on the interaction of RNA aptamer with graphene oxide," *RSC Advances*, vol. 9, pp. 19813–19818, 2019.